



This is a repository copy of *3D characterisation of indentation induced sub-surface cracking in silicon nitride using FIB tomography*.

White Rose Research Online URL for this paper:
<http://eprints.whiterose.ac.uk/148195/>

Version: Published Version

Article:

Baggott, A., Mazaheri, M. and Inkson, B.J. orcid.org/0000-0002-2631-9090 (2019) 3D characterisation of indentation induced sub-surface cracking in silicon nitride using FIB tomography. *Journal of the European Ceramic Society*, 39 (13). pp. 3620-3626. ISSN 0955-2219

<https://doi.org/10.1016/j.jeurceramsoc.2019.05.012>

Reuse

This article is distributed under the terms of the Creative Commons Attribution (CC BY) licence. This licence allows you to distribute, remix, tweak, and build upon the work, even commercially, as long as you credit the authors for the original work. More information and the full terms of the licence here:
<https://creativecommons.org/licenses/>

Takedown

If you consider content in White Rose Research Online to be in breach of UK law, please notify us by emailing eprints@whiterose.ac.uk including the URL of the record and the reason for the withdrawal request.



eprints@whiterose.ac.uk
<https://eprints.whiterose.ac.uk/>



Original Article

3D characterisation of indentation induced sub-surface cracking in silicon nitride using FIB tomography

A. Baggott^{a,*}, M. Mazaheri^b, B.J. Inkson^a^a NanoLAB, Department of Materials Science and Engineering, The University of Sheffield, Sheffield, S1 3JD, UK^b SKF Engineering & Research Centre, Kelvinbaan 16, 3439 MT, Postbus 2350, 3430 DT Nieuwegein, the Netherlands

ARTICLE INFO

Keywords:

Focused ion beam (FIB) tomography
 Silicon nitride
 Cracking
 Microindentation

ABSTRACT

In this study, a combination of 3D FIB tomography and incremental surface polishing has been used to characterize cracking beneath 0.5 kg and 1 kg Vickers indentations on silicon nitride. It is shown that a half-penny cracking regime exists even for low indentation loads with c/a ratios < 2 indicating that the c/a ratio cannot reliably be used to predict sub-surface crack morphology. For the first time, the presence of deep lateral cracks interconnected with radial cracks was also observed surrounding indentations of low loads on silicon nitride, and it is likely that these could contribute to material removal via spalling.

1. Introduction

Silicon nitride is an insulating, high hardness ceramic which has applications in the bearings industry within wind turbines and aircraft vehicles [1,2]. It is often used as an alternative to steel because it has a lower density, high electrical insulation, a higher hardness, and possesses good high temperature properties and oxidation resistance [3,4]. However, ceramics are intrinsically brittle, and it is therefore important to be able to characterise both the surface and sub-surface structure of defects formed during processing and service to predict how they behave under various external conditions.

The range of ceramic processing and service conditions under which defects form, and the variable nature of their morphology, make them difficult to investigate. However, microindentation of the material surface using a diamond tip can act as representative morphology for compression defects as they have similar characteristic features to lapping induced-indentations such as a residual central impression and a collection of surrounding cracks [5,6]. The applied load, as well as the geometry of the diamond tip, can also be varied to alter the morphology of the produced indent with one of the more common geometries used being the Vickers tip [7].

Surface imperfections can be effectively imaged using scanning electron microscopy (SEM) [8], optical microscopy, and white light interferometry [9]; although some additional preparation in the form of the addition of a conductive surface layer is usually required for SEM imaging when imaging insulators. Characterisation of sub-surface microstructure and crack morphologies however is more challenging and

methods with sufficient lateral and depth spatial resolution are limited. Serial-sectioning of Vickers indentations by manual grinding and subsequent SEM imaging has been undertaken [10,11] but this can require cracks to first be filled with a dye penetrant to increase visibility. In addition, incremental grinding and imaging is a time consuming process if multiple sections are desired, even more so if the imaging is carried out using an SEM (as transfer to and from the chamber is required in between grinding sections). Fluorescent dye has also been used to identify the location of sub-surface cracking, but does not provide information about crack depth, and assumes that cracks are fully saturated with penetrant [12,13].

Focused ion beam (FIB) tomography has emerged as a high-resolution serial sectioning technique for observing the sub-surface microstructure of samples; particularly in the area of defect analysis in materials science [14–19]. It involves the incremental slicing of material using a focused ion beam in order to reveal sequential cross-sections of the sub-surface, with each cross-section being imaged usually by a coincident electron beam. This allows for the generation of a 3D representation of the sub-surface via the collation and subsequent reconstruction of features within the individually imaged slices. Some of the original FIB tomography investigations were carried out with the aim of characterising crack morphologies beneath micro-indentations on non-conductive ceramic materials [17] and further studies produced 3D sub-surface crack maps of indentation zones [20–22]. Here, surface defects on silicon nitride have been modelled by Vickers micro-indentations of different applied loads, and characterised using both a surface-parallel diamond polishing method and FIB tomography in

* Corresponding author.

E-mail address: abaggott1@sheffield.ac.uk (A. Baggott).

order to reveal the nature of sub-surface cracking and how it relates to material removal mechanisms.

2. Materials and method

2.1. Material preparation

Two compositions of commercially available silicon nitride (ASTM F2094 certified hot isostatic pressed bearings-grade Si_3N_4 , supplied by SKF) were prepared for micro-indentation. These are denoted as SN-1 and SN-2. Both compositions possess a similar multiphase structure made up of isotropic alpha grains and needle-like beta grains with an intergranular amorphous phase. In both compositions the beta grains comprise > 95% of the microstructure. Samples were diamond polished down to a grit size of 1 μm (Minimet 1000) and indented using a diamond Vickers tip with loads of 0.5 kg and 1 kg with a 15 s dwell time (Struers Durascan).

2.2. Serial sectioning by incremental surface polishing

A polished SN-1 sample was Vickers indented three times with an applied load of 1 kg. The sample was then incrementally polished and optically imaged. Each increment of polishing was carried out (Minimet 1000) using 1 μm diamond paper with a force of 4 N, a speed of 25 rpm and a duration of 10 min. These parameters were chosen as they gave an appropriate material removal rate of 400–500 nm per increment. Indentations were optically imaged in both dark and bright field with a 50x objective lens (the 5 kg indentations were additionally imaged with a 20x lens to ensure they were within the FOV). Material removal rate was estimated by using an optical profiler (Bruker Contour GT) to measure the depth of a reference 5 kg indentation and its decrease in diagonal length with each polishing increment.

2.3. FIB tomography and SEM imaging

SEM and FIB tomography samples were mounted on SEM stubs and coated with a 30 nm layer of gold (Emscope SC500) to increase conductivity and reduce damage from the Ga^+ ion beam. FIB tomography on 0.5 kg and 1 kg Vickers indented samples was carried out using an FEI Helios NanoLab G3 DualBeam system. Surface images were obtained using FEG-SEM at 5 kV, a current of 1.6 nA and secondary electron (SE) imaging using an Everhart-Thornley detector (ETD). To access the sub-surface microstructure, first FIB step trenches were sputtered 20 μm away from the indentation sites on each of the

samples using 30 kV Ga^+ ions with a current of 65 nA. These trenches were subsequently polished using currents of 21 nA and 9.3 nA (Fig. 1(a)). FEI Autoslice and View software was used to incrementally sputter away slices of material with the FIB through the indentation sites. A current of 9.3 nA was chosen as the sputter rate was high enough to mill through the required volume of material whilst also obtaining a sufficient level of cross-section polishing. Each sputtered slice had approximate thickness $z = 750 \text{ nm}$ with cross-section dimensions $x = 40 \mu\text{m}$, $y = 30 \mu\text{m}$. The slice thickness was chosen as such to keep the experiment duration within a reasonable timescale (< days). The overall volume milled away around each indentation zone was $\sim 70,000 \mu\text{m}^3$. Sequential imaging of the milled cross-sections was carried out at a tilt angle of 52° with SEM SE images at 5 kV with a current of 1.6 nA. FIB ion-induced secondary electron (ISE) images were additionally taken at 30 kV and 9.3 nA after each mill, and drift was corrected for using a cross fiducial milled in to the surface of the sample. A schematic of the milling process is shown in Fig. 1(b).

For comparison, three whole indentations were milled: a 1 kg SN-1 indentation, a 1 kg SN-2 indentation, and a 0.5 kg SN-2 indentation. The direction of FIB milling approached towards the indentation corners in each case (as in Fig. 1(a)). In addition, to evaluate the importance of milling direction with respect to the indentation orientation, a second 1 kg SN-2 indentation was milled up to the indentation centre, but the approach angle was rotated by 45° to be towards one side of the indentation, not the corner.

3. Results

3.1. Micro-indentation of silicon nitride

For the SN-1 and SN-2 materials indented to 0.5 kg and 1 kg, the ratio of the surface radial tip-to-tip crack length, $2c$, to the indentation diagonal length, $2a$ (the c/a ratio) was calculated to be 1.7 for both compositions at 1 kg applied load, and 1.5 for the 0.5 kg SN-2 indentations (average of five indentations under each loads and composition). From the SEM cross-section images, the depths of the residual indent impressions that underwent FIB tomography were measured, from observing the SEM images of the FIB-milled cross-sections, to be $-2.6 \mu\text{m}$ and $-3.1 \mu\text{m}$ for the SN-2 0.5 kg and 1 kg indentations, and $-3.4 \mu\text{m}$ for the 1 kg SN-1 indentation. The Vickers hardness of the two compositions was $16.1 \pm 0.5 \text{ GPa}$ for SN-1 and $16.9 \pm 0.5 \text{ GPa}$ for SN-2.

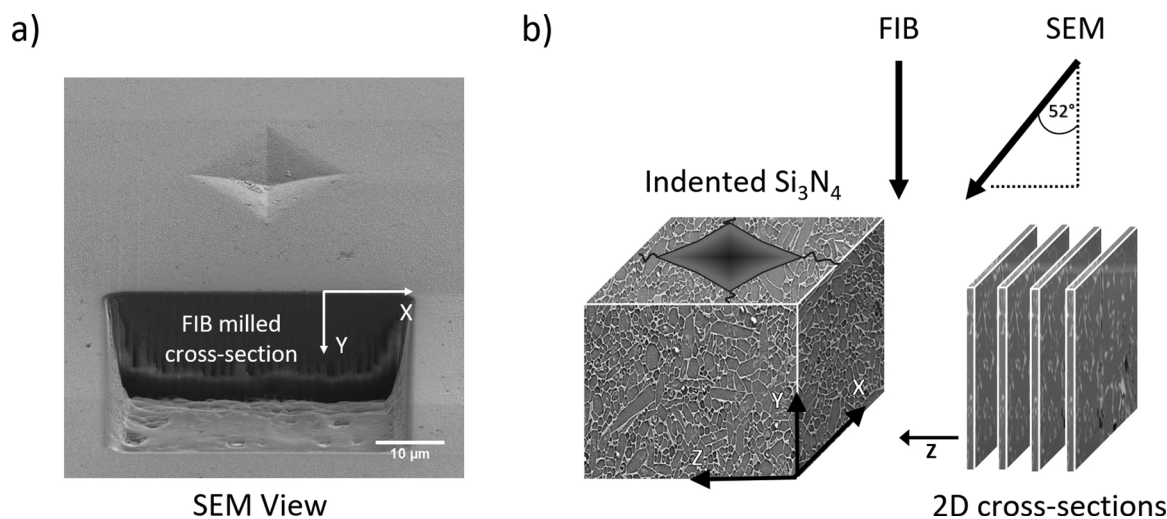


Fig. 1. (a) An SEM image with the 52° tilt showing a FIB milled cross-section adjacent to the indentation on the surface. (b) A schematic of the FIB-SEM milling process through an indentation: The FIB is used to mill away slices of material, after each slice the newly revealed cross-section is imaged using the SEM.

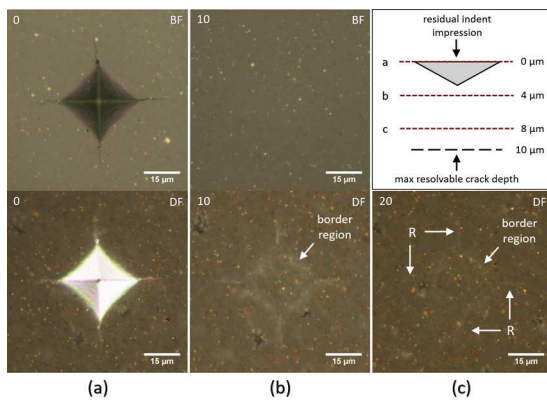


Fig. 2. Optical images in both bright field (top) and dark field (bottom) mode showing one of the 1 kg SN-1 indentations (a) before polishing (b) after the tenth increment of polishing, and (c) a schematic of where each image is in location to depth (top), as well as the dark field image after the twentieth increment.

3.2. Incremental polishing of indented SN-1

To investigate the influence of directional FIB serial sectioning on the observed 3D crack patterns, additional 1 kg indentations on the SN-1 composition were sectioned ‘top down’ by serial polishing and imaged optically. Fig. 2(a) shows dark and bright field images of one of the 1 kg indentations on the SN-1 sample prior to polishing. Radial cracks can be seen extending out from the indentation corners to a length of up to 10 μm . No lateral cracking was observed in images of the 1 kg indentations prior to polishing (Fig. 2(a)). After ten polishing increments, the central residual indentation impression and radial cracks of the 1 kg indentations were no longer visible in bright field mode (as shown in Fig. 2(b)). However, under dark field the radial cracks are visible as well as a border zone (arrowed) surrounding where the residual indent impression previously was. The visible border zone scatters light in the same manner as the radial cracks, which suggests that it may consist of localized micro-cracking or a region of high dislocation density plastically deformed zone [23].

As the polishing depth increased, the visibility of the 1 kg indentation features decreased. This is particularly evident for the radial cracks seen in Fig. 2(c) after the twentieth polishing increment (a depth of -8 μm). The maximum depth at which features of the 1 kg indentations were resolvable by optical microscopy was after the twenty-fourth increment, i.e. a depth of -10 μm . Both the light scattering border region and the radial cracking were present at the maximum resolvable depth with the radial cracks being connected to the border at all depths.

3.3. D FIB tomography of micro-indentations

3.3.1. FIB sectioning of 1 kg SN-1 indentation

Fig. 3 gives examples of electron induced secondary electrons (ESE) imaged cross-sections of the 1 kg SN-1 sample at increasing proximity to the indent zone. In Fig. 3(a) a radial crack can be seen emanating to a depth of 20 μm beneath the surface. The jagged pathway of the crack suggests that cracking is intergranular in nature. As the milling approaches the indentation corner (Fig. 3(b)) crack branching occurred and a lateral crack appeared emanating from the sub-surface radial crack at a depth of -11 μm and an angle of -15° relative to the surface plane. This was later followed by a second lateral branching from the other side of the radial at the same depth and an angle of -19°. The cross-section in Fig. 3(c), shows that as the indentation corner is passed, and milling progresses to the residual indentation impression, the radial crack sectioned here (Fig. 3(a, b)) does not extend further under the residual indentation impression, whereas the lateral exists under this central zone. For some lateral cracks it was not possible to measure

their full dimensions in a given x–y cross-section plane if they extended sideways past the milled trench wall.

The lateral cracks observed in Fig. 3(c) disappeared as FIB sectioning approached the mid-point between the already milled indentation corner and the centre of the indentation. In Fig. 4, the presence of a radial crack parallel to the mill direction emanating from one of the indentation corners is observed as a damaged region exhibiting interconnected micro-cracking. It is difficult to determine the depth of parallel radial cracks as their crack width and/or width of crack path is of the order of the FIB slice width. Directly beneath the centre of the residual indentation impression, but not intersecting with the surface, cracking is observed starting at a depth of -20 μm and extending to a minimum depth of -30 μm ; this type of cracking that has no intersection with the surface plane and extends beneath the residual indentation impression (arrowed in Fig. 4) has been determined here as half-penny cracking [11,24]. In the region directly below the residual indentation impression, there exists a crack free-zone where no cracking was observed.

It should be noted that in all the SE imaged cross-sections shown in Fig. 3, the milled trenches have a build-up of material (lighter contrast) located on the side walls as well as at the bottom of the trench caused by redeposition of sputtered material. Sputtered material can not only obstruct the view of the cross-section, but also has the potential to redeposit within cracks and hence decrease their visibility. In addition, there is also a variation in brightness across the face of the cross-sections due to different levels of SE emissions resulting from localised charge build-up on the insulating silicon nitride surface; this is particularly prominent around cracking (Fig. 3). The shadowing effect near the side and bottom of the trenches in Fig. 3 is caused by the presence of the trench walls that inhibit the SE from reaching the detector. These phenomena are highlighted in Fig. 3(d).

3.3.2. Effect of load and material

The cracking observed at 1 kg load in SN-1 was compared to that induced by the same 1 kg load in the SN-2 material. The SN-2 1 kg indented sample showed a very similar cracking morphology with lateral cracks visible in the vicinity of the sectioned indentation corner at a maximum depth of -17 μm and angle 28°. Half-penny cracking was also observed beneath the central indentation starting at a depth of -23 μm extending to -30 μm as in the SN-1 sample. For both the SN-1 and SN-2 1 kg indented samples, the extent of cracking observed during the second half of indentation milling was significantly less than in the first. Only radial cracks were visible (no laterals) and these were identified at a lesser depth and with a reduced crack width in comparison to the first half of the indentation.

The cracking observed around 1 kg indentations was compared to that occurring around a lower load 0.5 kg SN-2 indentation. Crack depths and sizes were all reduced as the indentation load was decreased from 1 kg to 0.5 kg. For the 0.5 kg indented SN-2 sample, lateral cracks were still observed on approach to the indentation corner at a maximum depth of -9 μm , which is consistent with a reduced depth compressive stress zone. Half penny cracking was visible starting -14 μm below the centre of the indentation extending to a depth of -20 μm . Unlike in the 1 kg indentations, radial cracking was not detected in the second milling half for the 0.5 kg indentation.

3.3.3. Effect of FIB sectioning direction

To investigate the role of FIB sectioning direction on the observed crack morphologies a 1 kg indentation in SN-2 was sectioned parallel to the indentation side. In SEM cross-section images of the 1 kg SN-2 indentation where the milling was towards the indentation side (not the corner as in the previous mills), two radial cracks emanating from the closest two indentation corners were visible sub-surface. The orientation of these radials is expected to be -45° to the sectioning FIB plane. On approach to the edge of the residual indentation impression, these radials became shallower and interconnected with shallow micro radials

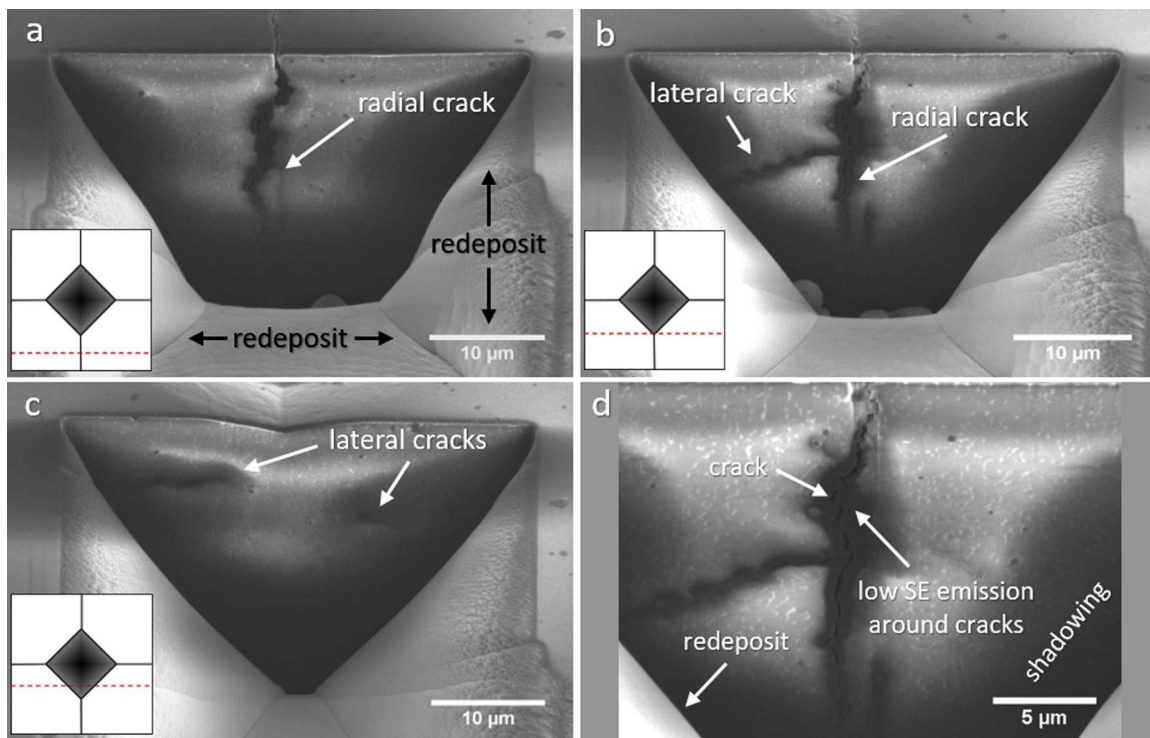


Fig. 3. SEM imaged cross-sections of the 1 kg SN-1 FIB-milled indentation taken at a tilt angle of 52°. The inset schematics in the bottom left show the cross-section location in relation to the indentation: (a) FIB slice through the radial crack (arrowed) emanating from an indentation corner. (b) Slice taken at the indentation corner showing both lateral and radial cracking. (c) Approaching the indentation center where lateral cracking is observed. (d) A close up of the cross-section in (b) Strong variations in SE contrast is due to localized voltage contrast (charging) and beam shadowing caused by the trench walls.

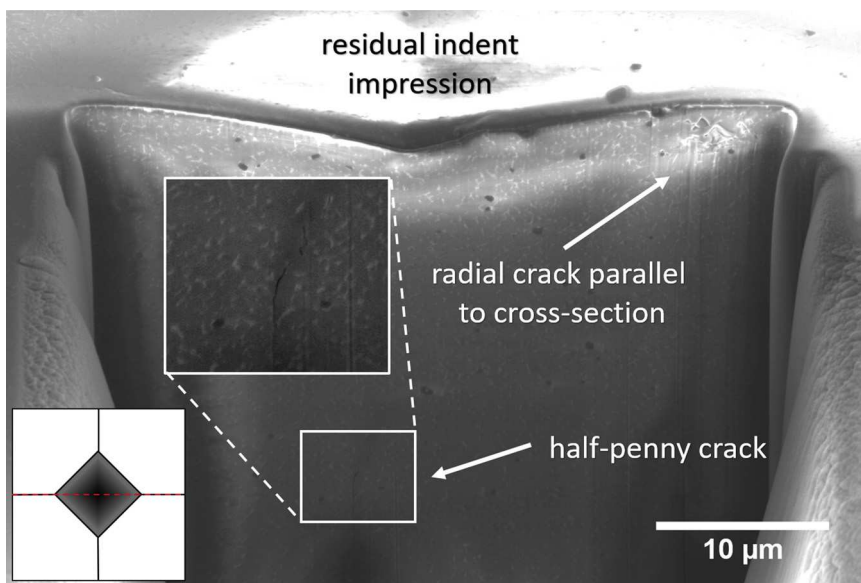


Fig. 4. An SEM imaged FIB cross-section through the centre of the 1 kg SN-1 indentation (sectioned in Fig. 3) taken at a tilt angle of 52°. A radial crack occurring predominantly parallel to the milling direction and a central half-penny crack (magnified inset) are identified.

as highlighted in Fig. 5. In addition, near the indentation edge, deep laterals were identified at a maximum depth of -14 μm, as well as micro-cracking near the surface (arrowed Fig. 5). There was also evidence in one cross-section of half-penny cracking, observed beneath the indentation centre at a depth of -16 μm.

4. 3D crack map analysis and discussion

4.1. 3D FIB tomographic crack reconstructions

3D reconstructions of the cracks identified in the SE imaged FIB cross-sectioned slices through indentations were carried out using IMOD software for both SN-1 and SN-2 samples to produce sub-surface crack maps of the FIB milled volumes. Fig. 6(a, b) shows the crack maps for the SN-2 0.5 kg and 1 kg indentations overlaid onto SEM images of

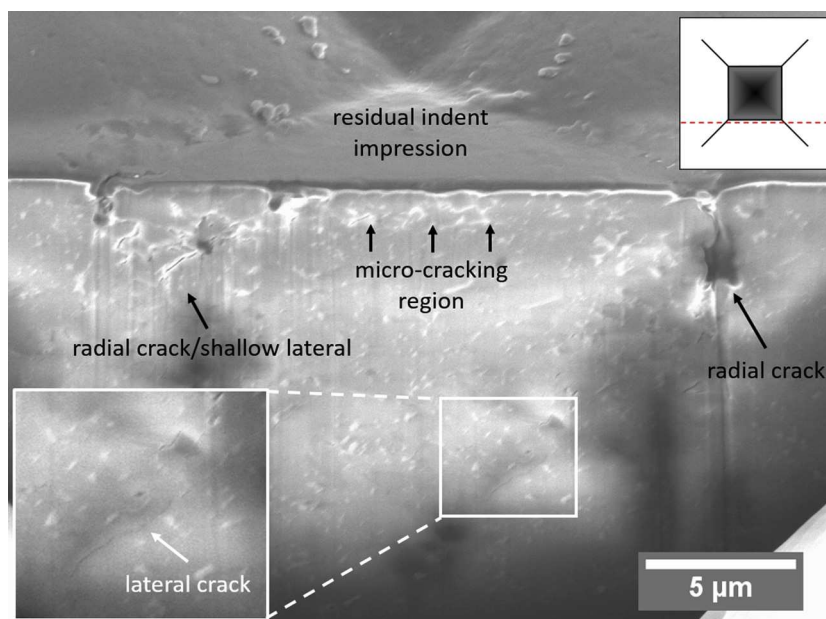


Fig. 5. An SEM imaged (tilt angle of 52°) FIB cross-section located at the edge of the 1 kg SN-2 indentation where the FIB milling approach was towards the indentation side. Two radial cracks are visible in addition to sub-surface micro-cracking along the indentation edge, and deep lateral cracking.

the indentations at a 52° tilt angle. Lateral and radial cracking is coloured blue and red respectively.

The sub-surface crack maps for the 0.5 kg and 1 kg indentations exhibit a similar morphology when FIB milled towards an indent corner, with an initial radial crack first identified followed by secondary laterals on approach to the residual indentation impression. Both loads also showed evidence of half-penny cracking as opposed to the Palmqvist morphology often predicted for Vickers indentations where the crack length (c)-to-indent half diagonal (a) ratio is < 2 [11,25,26]. The c/a ratio was measured here as 1.5 for the 0.5 kg indentation and 1.7 for the 1 kg indentation so half-penny cracking in the 1 kg indentation is not unexpected, however it is more surprising for the 0.5 kg indentation. It may be that half penny cracking has not been identified in Vickers indentations of lower loads due to their small crack width in addition to the limitations of the techniques used [10,11]. The geometry of half-penny cracking observed in the FIB milled indentations was vertically oriented along the principle stress axes, i.e. the diagonals of the indentation.

The crack density in the first half of the indentations is greater than

that observed in the second half, with no lateral cracks observed in the second half under 0.5 kg and 1 kg indentation loads, and radial cracks only observed in the second half for the 1 kg indentation. The observed change in crack density can be explained by the localised changes in stress as a result of FIB milling ([20,27]). Cracks are originally formed as stress relief mechanisms to counteract the high compressively stressed plastically deformed zone beneath the residual indentation impression formed during loading. As the indentation is milled through and the plastically deformed zone sputtered away, the associated tensile and compressive stresses are also reduced causing the remaining cracks to close, hence making them harder to resolve under SEM.

The depth of half-penny cracks beneath indentations, and their pathway, can be used as an indicator of the volume that the plastically deformed zone occupies. Cracks do not preferentially propagate into the plastically deformed zone due to the increased hardness high compressive stress present [10], although micro-cracking can exist in this zone [18]. Instead the crack pathway traces around the tensile stress region surrounding the deformation zone resulting in the half-penny cracking. In Fig. 7(a, b) side-on views of the IMOD crack maps

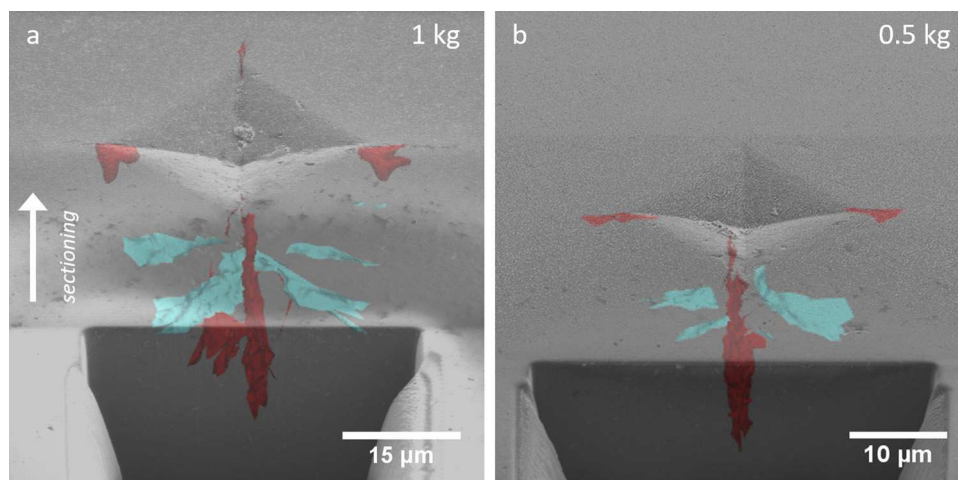


Fig. 6. Crack maps created using IMOD overlaid onto SEM images taken at a 52° tilt angle for the SN-2 (a) 1 kg indentation and (b) 0.5 kg indentation. Lateral cracks are coloured blue and radial cracks red (For interpretation of the references to colour in this figure legend, the reader is referred to the web version of this article).

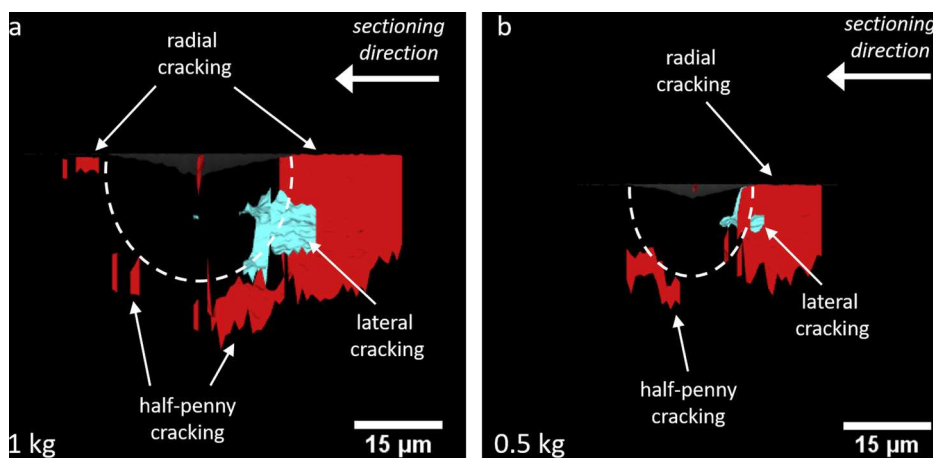


Fig. 7. Side view schematics of the sub-surface IMOD crack maps for the SN-2 (a) 1 kg indentation, and (b) 0.5 kg indentation highlighting the location of the different crack morphologies (arrowed). Lateral and radial cracks are coloured blue and red respectively. The region of compressive stress beneath each indentation is highlighted by the dashed semi-circle (For interpretation of the references to colour in this figure legend, the reader is referred to the web version of this article).

for the 0.5 kg and 1 kg SN-2 indentations are given, there is a hemispherical volume below the indentations (dashed line) with radius $-12\ \mu\text{m}$ and $-17\ \mu\text{m}$ respectively where there is minimal cracking; this is the volume taken up by the plastically deformed zone and equates to volumes of $-3000\ \mu\text{m}^3$ and $-11,000\ \mu\text{m}^3$.

In previous studies of Vickers indentations on silicon nitride using sectioning via incremental polishing and flexure breaking [10,11], lateral cracking was not observed at applied loads of 1 kg whereas here lateral cracking was observed in all four FIB milled indentations using the higher spatial resolution SEM method. A manual grinding study on silicon nitride [10] which utilised SEM imaging with dye penetrant to increase the contrast of cracks only showed lateral cracking for indentation loads $> 3\ \text{kg}$, although this assumes the cracks are fully saturated which they may not have been. However, sub-surface lateral cracking beneath the indentation corner for indentation loads of 0.5 kg and 1 kg has been detected via SEM imaging of FIB-milled single cross-sections in other polycrystalline ceramics [19,28]. The presence of lateral cracking observed here could be initiated or opened wider by the stress changes associated with FIB milling in a similar manner to the crack closure than occurs in the second half of the indentation. When first FIB milling towards the indentation, the surface radial crack can propagate towards the milled trench, hence increasing the surface length as well as the crack tip width; this phenomenon was seen when milling towards an indentation corner but not when the milling direction was 45° to the indentation corner. The opening of a new free-surface in the form of the FIB milled trench inevitably changes the residual stress levels, which may cause a change in the opening of the cracks [20]. Time-dependent changes in sub-surface lateral crack geometries were not observed during this study.

Considering the influence of crack milling direction, Fig. 8 shows the 3D crack map of the SN-2 1 kg indentation milled 45° to the indentation corner. There are both shallow (depth $< 5\ \mu\text{m}$) and deeper

(depth $> 5\ \mu\text{m}$) lateral cracks surrounding the indentation. The shallow laterals were observed to be related to near-surface micro-cracking at the edge of the residual indentation impression and connected to radial cracks at the point they intersect with the surface (as seen in Fig. 5). These shallow laterals would be susceptible to propagation and material removal via chipping and flaking if high contact pressures were to be applied during operation conditions [29,30].

Both the shallow and deep laterals are located adjacent to the central indentation damaged zone, with the deeper laterals existing deep under the residual indentation impression/high compressive stress zone as seen in Figs. 6–8. The majority of the lateral cracks do not intersect the surface, however, there is evidence from the FIB sectioning that the lateral cracks frequently connect to adjacent radial cracks sub-surface (Fig. 8). Unlike in an investigation of lateral cracks generated by indentations of greater applied loads ($> 3\ \text{kg}$) [10], the lateral cracks observed here do not extend outwards from the indent centre to intersect with the tips of radial cracks. In a similar way to how half-penny cracks trace around the edge of the central plastically deformed/compressive stress zone (Fig. 7), the location and inner boundaries of the deep laterals also indicate the depth of this zone. The presence of half-penny cracks and laterals that are located at some depth beneath an indentation's surface could lead to significant material removal via spalling under applied pressure.

4.2. Incremental surface polishing

The resolution of dark field optical imaging was sufficient to detect radial cracks and an optical contrast zone bordering the edge of the residual indentation impression. The incremental polishing of the SN-1 1 kg indentations did not show any evidence of lateral cracking before or during polishing, which may be because the sub-surface lateral cracking was located adjacent to, within and under the micro-cracking

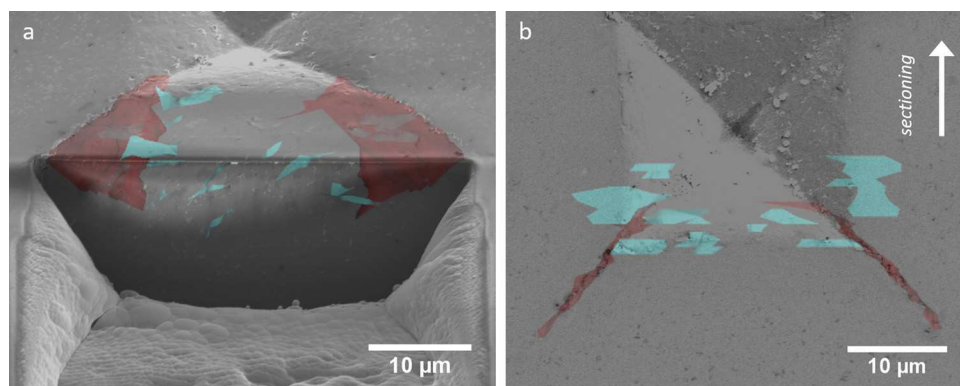


Fig. 8. Crack maps made in IMOD overlaid on to SEM images for the 1 kg SN-2 indentation that was milled towards the indentation side. (a) 52° view of the indentation (b) Top down view of the indentation. Lateral and radial cracks are colored blue and red respectively (For interpretation of the references to colour in this figure legend, the reader is referred to the web version of this article).

region surrounding the residual indentation impression and hence was difficult to resolve. This is supported by the FIB tomography results that revealed micro-cracking in the same region as the deep laterals. In addition, because the laterals are near parallel to the sample surface (0–28°), it is likely that they are removed by the polishing process in between imaging steps, as their dimensions are of the same order as the polishing increments.

The morphology of the radial cracks identified by incremental polishing was consistent with a half-penny crack regime, due to the unchanging morphology of the radial cracks with polishing depth. In a Palmqvist regime, it would be expected that the radial cracks would detach from the indentation corners with depth, but this was not seen either by optical or FIB-SEM imaging.

The decrease of crack visibility with depth (–10 µm) in the optical observations is most likely due to the radial crack opening width decreasing below the spatial resolution of the optical microscope which requires crack openings to be wide enough for light scattering to occur and enough of the scattered light to be detected. Crack width decreases with depth anyway however, further crack closure may have occurred here as a result of the polishing away of the compressively stressed plastically deformed volume that exists beneath the residual indentation impression. Surrounding this is a zone of high tensile stress that causes the initiation of the radial cracks as a stress relief mechanism. When the compressive zone is removed by the polishing, the surrounding tension will reduce, and the cracks are no longer acting to alleviate stress and therefore close; this is similar to the mechanism behind the crack closure seen in the second half of the FIB-milled indentations.

5. Conclusion

Sub-surface cracking in Vickers microindentations on silicon nitride has been investigated in 3D using FIB tomography and incremental surface-parallel polishing. Both methods showed evidence of half-penny cracking for 1 kg applied indentation loads. FIB tomography, for the first time, also revealed unexpected half-penny cracking also for indentations of lower loads (0.5 kg with a c/a ratio-1.5) where a half-penny cracking regime had not been observed in previous investigations using alternative methods. FIB tomography also reveals deep laterals interconnecting with the radial cracks surrounding the residual indentation impression for both loads; this has only been observed at such low indentation loads in one previous study in a related ceramic material. These half-penny and deep lateral cracks originate at the region where the plastically deformed zone transitions to the bulk phase.

The discovery of sub-surface half-penny and lateral cracking in low load Vickers indentations, with c/a ratios as low as 1.5 is not only important for how the c/a ratio is used as an evaluation parameter for sub-surface cracking regimes, but also in the understanding of how crack systems on silicon nitride material may further evolve under operation conditions. In addition, FIB tomography for sub-surface microscale defect characterisation has proved to be more effective than previous methodologies.

Declarations of interest

None.

Author contributions

Adam Baggott – Responsible for the sample preparation, collection of data using FIB-SEM, analysis of data, and writing the bulk of the manuscript.

Mehdi Mazaheri – Provision of silicon nitride samples in addition to offering expertise on the material and indentation analysis.

Beverley Inkson – Conceived of presented idea and supervision of the project. Assistance in writing the manuscript.

Acknowledgments

The authors gratefully acknowledge the support of the Engineering and Physical Sciences Research Council (EPSRC) for a PhD studentship (A. Baggott) grant, EP/M508135/1.

References

- [1] R. Raga, I. Khader, C. Zdeněk, A. Kailer, Experimental and numerical investigation of crack initiation and propagation in silicon nitride ceramic under rolling and cyclic contact, *J. Phys. Conf. Ser.* 843 (1) (2017).
- [2] L. Wang, R. Snidle, L. Gu, Rolling contact silicon nitride bearing technology: a review of recent research, *Wear* 246 (1–2) (2000) 159–173.
- [3] S. Hampshire, Silicon nitride ceramics - review of structure, processing and properties, *J. Achiev. Mater. Manuf. Eng.* 24 (1) (2007) 43–50.
- [4] Z. Krstic, V.D. Krstic, Silicon nitride: The engineering material of the future, *J. Mater. Sci.* 47 (2) (2012) 535–552.
- [5] K. Kida, T. Urakami, T. Yamazaki, K. Kitamura, Surface crack growth of silicon nitride bearings under rolling contact fatigue, *Fatigue Fract. Eng. Mater. Struct.* 27 (2004) 657–668.
- [6] M. Hadfield, T.A. Stolarski, Observations of delamination fatigue on pre-cracked ceramic elements in rolling contact, *Ceram. Int.* 21 (2) (1995) 125–130.
- [7] R. Cook, G. Pharr, Direct observation and analysis of indentation cracking in glasses and ceramics, *J. Am. Ceram. Soc.* 73 (4) (1990) 787–817.
- [8] K. Kida, M. Saito, K. Kitamura, Flaking failure originating from a single surface crack in silicon nitride under rolling contact fatigue, *Fatigue Fract. Eng. Mater. Struct.* 28 (12) (2005) 1087–1097.
- [9] J.J. Yu, W.M. Guo, W.X. Wei, H.T. Lin, C.Y. Wang, Fabrication and wear behaviors of graded Si₃N₄ ceramics by the combination of two-step sintering and β-Si₃N₄ seeds, *J. Eur. Ceram. Soc.* 38 (10) (2018) 3457–3462.
- [10] T. Lube, Indentation crack profiles in silicon nitride, *J. Eur. Ceram. Soc.* 21 (2001) 211–218.
- [11] H. Miyazaki, H. Hyuga, Y. ichi Yoshizawa, K. Hirao, T. Ohji, Crack profiles under a Vickers indent in silicon nitride ceramics with various microstructures, *Ceram. Int.* 36 (1) (2010) 173–179.
- [12] H. Fischer, F. Karaca, R. Marx, Detection of microscopic cracks in dental ceramic materials by fluorescent penetrant method, *J. Biomed. Mater. Res.* 61 (1) (2002) 153–158.
- [13] C. Vieillard, Observation of subsurface rolling contact fatigue cracks in silicon nitride and comparison of their location to Hertzian contact subsurface stresses, *Int. J. Fatigue* 96 (2017) 283–292.
- [14] P.R. Munroe, The application of focused ion beam microscopy in the material sciences, *Mater. Charact.* 60 (1) (2009) 2–13.
- [15] N. Bassim, K. Scott, L.A. Giannuzzi, Recent Advances in Focused Ion Beam Technology and Applications, (2017), pp. 317–325.
- [16] L.A. Giannuzzi, F.A. Stevie, Introduction to Focused Ion Beams: Instrumentation, Theory, Techniques and Practice, Springer Science & Business Media, 2006.
- [17] B.J. Inkson, T. Steer, H.Z. Wu, G. Möbus, 3D mapping of subsurface cracks in alumina using FIB, *Mater. Res. Soc. Symp. - Proc.* 649 (2001) Q7.7.1–Q7.7.6.
- [18] H.Z. Wu, S.G. Roberts, G. Möbus, B.J. Inkson, Subsurface damage analysis by TEM and 3D FIB crack mapping in alumina and alumina/5vol.%SiC nanocomposites, *Acta Mater.* 51 (1) (2003) 149–163.
- [19] Z.H. Xie, P.R. Munroe, R.J. Moon, M. Hoffman, Characterization of surface contact-induced fracture in ceramics using a focused ion beam miller, *Wear* 255 (1–6) (2003) 651–656.
- [20] F. Elfallagh, B.J. Inkson, Evolution of residual stress and crack morphologies during 3D FIB tomographic analysis of alumina, *J. Microsc.* 230 (Pt. 2) (2008) 240–251.
- [21] F. Elfallagh, B.J. Inkson, 3D analysis of crack morphologies in silicate glass using FIB tomography, *J. Eur. Ceram. Soc.* 29 (2009) 47–52.
- [22] N. Payraudeau, D. McGrouther, K.U. O’Kelly, Quantification of subsurface damage in a brittle insulating ceramic by three-dimensional focused ion beam tomography, *Microsc. Microanal.* 17 (2) (2011) 240–245.
- [23] E.W. Roberts, P.C. Robinson, Light microscopy of ceramics, *J. Microsc.* 140 (2) (1985) 137–158.
- [24] Y. Tang, A. Yonezu, N. Ogasawara, N. Chiba, X. Chen, On radial crack and half-penny crack induced by Vickers indentation, *Proc. R. Soc. A Math. Phys. Eng. Sci.* 464 (May) (2008) 2967–2984.
- [25] X. Yang, X. Liu, Z. Huang, X. Yao, G. Liu, Vickers indentation crack analysis of solid-phase-sintered silicon carbide ceramics, *Ceram. Int.* 39 (1) (2013) 841–845.
- [26] K. Niihara, A fracture mechanics analysis of indentation-induced Palmqvist crack in ceramics, *J. Mater. Sci. Lett.* 2 (5) (1983) 221–223.
- [27] B.J. Inkson, D. Leclere, F. Elfallagh, B. Derby, The effect of focused ion beam machining on residual stress and crack morphologies in alumina, *J. Phys. Conf. Ser.* 26 (1) (2006) 219–222.
- [28] Z.H. Xie, M. Hoffman, R.J. Moon, P.R. Munroe, Y.B. Cheng, Subsurface Indentation Damage and Mechanical Characterization of α-Sialon Ceramics, *J. Am. Ceram. Soc.* 87 (11) (2004) 2114–2124.
- [29] Y. Wang, M. Hadfield, A study of line defect fatigue failure of ceramic rolling elements in rolling contact, *Wear* 253 (9–10) (2002) 975–985.
- [30] Y. Wang, M. Hadfield, A mechanism for nucleating secondary fractures near a pre-existing flaw subjected to contact loading, *Wear* 254 (7–8) (2003) 597–605.